Hindawi
Advances in Civil Engineering
Volume 2020, Article ID 4936342, 10 pages
https://doi.org/10.1155/2020/4936342

Research Article

Effect of the Concrete Mesostructure Geometric Form on Its Elastic Modulus

Xu Yang [1,2,3]

[1]*School of Civil Engineering, Harbin Institute of Technology, Harbin 150090, China*
[2]*Key Lab of Structures Dynamic Behavior and Control of the Ministry of Education, Harbin Institute of Technology, Harbin 150090, China*
[3]*Key Lab of Smart Prevention and Mitigation of Civil Engineering Disasters of the Ministry of Industry and Information Technology, Harbin Institute of Technology, Harbin 150090, China*

Correspondence should be addressed to Xu Yang; yangxu_phdce@mail.com

Received 30 August 2019; Revised 28 November 2019; Accepted 13 January 2020; Published 10 February 2020

Academic Editor: Xuemei Liu

A comprehensive understanding of the geometrical form of the concrete mesostructure is important because it is associated with the complex and random mechanical behavior of the concrete. There is still uncertainty about how to characterize the geometrical form of the concrete mesostructure and its effect on the observed macroscopic behavior. The coarse aggregate content and fractal dimension were used in this study to indicate the geometrical form of concrete at the mesolevel. Taking the mechanical parameters measured in experiments, a group of mesomodels with various fractal dimensions and coarse aggregate contents was simulated by using the random fractal modeling method and then was studied and discussed. The analytical solution, simulation, and experimental data all suggested that the elastic modulus increased with the increasing coarse aggregate content. Meanwhile, the fractal dimension can cause the elastic modulus to decline slightly. The comprehensive consideration of both fractal geometry and classical Euclidean geometry can aid in predicting the macroscopic behavior of concrete.

1. Introduction

There is little doubt nowadays that the macroscopic behavior of concrete is strongly influenced by the geometrical and mechanical properties of its components at the mesolevel and that analyzing the materials at that level is an extremely powerful tool for understanding and predicting the observed macroscopic behavior. The study at the mesolevel is followed by a variety of models and approaches. In some of them, the mesostructure is represented via continuum finite elements which discretize separately the larger aggregates and the matrix (including mortar, smaller/fine aggregates, and air voids with the hardened cement paste), with or without the representation of material interfaces [1].

These models and approaches could be solved by various analytical and numerical methods. As compared to analytical methods, the numerical methods have a wider range of applications. Besides, the numerical mesomodeling method of concrete is not limited by the experimental equipment or sites, based on which the results can be obtained conveniently and precisely. The researchers just need to establish a reasonable mesomodel of concrete and assign material properties of each component. Then, this numerical model can help us to study the influence of components on the mechanical behavior of concrete.

In the theoretical frame of concrete mesomechanics, many numerical methods were developed. Zhang considered that different mesoscopic numerical methodologies are similar [2]. The key step of all the methods was to assume the mesostructure and components of concrete logically before the analysis. Not only the mechanical properties of components but also the geometrical form of their mesostructure can influence the mechanical behavior of concrete. However, there is a lack of discussion on the geometrical form of the concrete mesostructure. Characterizing the geometrical form of the concrete mesostructure and its influence on the

macroscopic behavior is an important, but understudied, cause for concern.

With the quantitative analysis method for characterizing the geometrical form of the concrete mesostructure developed [3–7], several correlations between the macroscopic behavior of concrete and the geometrical parameters of its mesostructure were then revealed. It was demonstrated that the coarse aggregate content (CAC) can influence the compressive and tensile strength [8], the elastic modulus [9], the thermal properties [10], the chloride diffusivity in concrete [11–13], etc. Additionally, some other geometrical parameters can also influence the macroscopic behavior of concrete. For instance, the aggregates' gradation affects the compressive strength [14]. Young's modulus of concrete decreases with the increase of the ITZ thickness [15]. The stress state of localized areas is influenced by the spatial distribution of aggregates [16]. The critical crack-tip opening displacement and toughness fracture can be predicted more precisely considering the maximum aggregate size and aggregate type (river or crushed) [17]. The needle flake coarse aggregate particles cause uneven distribution of the concrete equivalent elastic modulus [18]. With more detailed studies on concrete mesomechanics, some researchers pointed out that the influence of the random spatial distribution of aggregates in concrete on the simulation and experimental results should never be neglected [4, 19–22].

However, all the studies introduced above did not find an advisable indicator that could describe the complicated and random spatial distribution of aggregates. Some discussions of the geometrical form character were constructed on a few assumptions made by the researchers. In several studies, the aggregates were simulated as spheres or ellipses simplistically. Some researchers considered that each distribution was different. Moreover, some other researchers considered the gradation of aggregates, e.g., the two-gradation or the full-gradation, as an indictor semiquantitatively. Subsequent research has confirmed that the geometrical parameters in the theoretical frame of classic Euclidean geometry could only characterize a part of the geometrical form of the concrete mesostructure. Although these studies did not establish a quantitative model that could completely describe the correlation between the macroscopic behavior of concrete and the geometrical parameters of its mesostructure, these works provided a research foundation.

The fractal dimension was introduced into the study of the concrete mesostructure, which was efficient to quantify the irregular objectives [23–25]. The word "fractal" was coined by B. B. Mandelbrot from the Latin adjective to describe the fragmented, irregular, random, and scaled pattern he studied [26]. Based on the determination of the fractal dimension, previous researches succeeded in establishing the relationship between the fractal dimension and several macroscopic behaviors of concrete. For instance, it was demonstrated that the higher fractal dimension indicates a tougher surface [27]. Then, the relationship between fracture energy and fractal dimension of crack could be given [28–30].

These studies have shown the beneficial effects of applying fractal dimension in the research of concrete at the mesolevel. Otherwise, most studies in this field have only focused on analyzing the surface or other two-dimensional objectives. There is still uncertainty about how to characterize the geometrical form of the concrete mesostructure and its influence on the macroscopic behavior.

In our previous works, it was demonstrated that the fractal dimension of aggregates in concrete is a constant equal to three, and the dimension of the matrix should be a positive real number less than three [31]. Then considering the shape, the size, and the spatial distribution of aggregates, an approaching model of the concrete mesostructure was proposed. Based on these theoretical foundations, an accurate and efficient numerical modeling method of the concrete mesostructure, random fractal modeling (RFM) method, was introduced.

In this paper, an analytical-method-based elastic modulus prediction was discussed. A qualitative result of how the elastic modulus was influenced by the CAC was obtained. Furthermore, with a comprehensive consideration of the fractal geometry and classic Euclidean geometry, the effect of geometrical form parameters, i.e., the fractal dimension of the concrete mesostructure and the CAC, on the elastic modulus of concrete was quantitatively studied.

2. Methods

2.1. Geometric Form of the Concrete Mesostructure. Concrete is commonly considered a three-phase composite on the mesoscale, consisting of the aggregates, the matrix, and the interface transition zone (ITZ) between these two. Specifically, the aggregate only represents the larger aggregate piece in this study, which is approached as a polyhedron model. The aggregates are embedded in a matrix phase representing mortar plus the smaller aggregates and the air voids.

Especially, the ITZ has an obvious effect on the macromechanical behavior of concrete, and thus, it should be included in investigations of the mechanical properties of concrete. However, the thickness of the ITZ is considered to be between 15 and 40 μm [32, 33] in general, which is much smaller than the size of the aggregate particles. Therefore, when investigating the geometric and fractal characteristics of the concrete mesostructure, the ITZ can be neglected.

In the geometric model that neglects the ITZ, concrete is denoted as the set $\mathscr{F}$, the aggregates as the set $\mathscr{G}$, and the matrix as the set $\mathscr{H}$. Thus, sets $\mathscr{G}$ and $\mathscr{H}$ are proper subsets of the set $\mathscr{F}$. Moreover, the set $\mathscr{G}$ is the relative complement of $\mathscr{H}$ in the set $\mathscr{F}$. Both aggregates (set $\mathscr{G}$) and matrix (set $\mathscr{H}$) typically represent fractal features, although their dimensions differ. Our previous work demonstrated that the dimension of the set $\mathscr{G}$ is a constant integer equal to three. Meanwhile, the fractal dimension of the set $\mathscr{H}$ is a positive real number less than three, and its specific value should be determined by measurement or calculation. It is influenced by the gradation and spatial distribution of the aggregates.

With the aid of X-ray computed tomography and sieving tests, the fractal dimension of a matrix can be determined using the box-counting method. More details regarding

these determination methods and a discussion of fractal dimension can be found in [31].

Based on the fractal dimension of the matrix, it is possible to describe the fractal, random, and complicated geometric features quantitatively. Generally, a higher fractal dimension indicates greater geometrical complexity [26, 34–36]. Thus, the geometric forms of concrete samples or numerical models can be distinguished by their fractal dimensions. Furthermore, according to the fractal theory, if the fractal dimensions of the two sets are equal, these sets can be considered "the same fractal set" [37]. Based on this property, a random-fractal-based concrete mesosimulation method can be formulated as follows: using an iterative modeling algorithm, a geometric pattern is generated to have the same fractal dimension as that of an actual concrete sample, and this pattern can be considered a numerical model having the same fractal and geometric features as the actual concrete sample [38]. This simulation method is discussed in more detail in Section 2.3.1.

By applying the analytical method, simulation, and experimentation, two parameters of the concrete geometric form would be studied, i.e., the CAC and the fractal dimension of the matrix.

2.2. Analytical-Method-Based Elastic Modulus Prediction. It has been demonstrated that the influence of the ITZ on the elastic modulus should not be neglected [39]. The equations considering the ITZ could not be solved analytically. The prediction of elastic modulus based on the analytical method would not include the ITZ between the aggregate and the matrix simplistically in this study.

2.2.1. Idealized Homogeneous Strain and Stress Boundary Conditions. The idealized homogeneous strain boundary condition was assumed. The field of a representative volume element of concrete is denoted as Ω. Based on the principle of minimum potential energy and the principle of minimum complementary energy, the upper and lower bounds of the equivalent elastic modulus L of Ω can be given as the following inequations:

$$\begin{aligned}\overline{U} &\le \frac{1}{2|\Omega|}\int_{\Omega} L_{ijkl}\epsilon'_{kl}\epsilon'_{ij}dV,\\ \overline{U} &\ge E_{ij}\frac{1}{|\Omega|}\int_{\Omega}\sigma^{*}_{ij}\mathrm{d}V - \frac{1}{2|\Omega|}\int_{\Omega} H_{ijkl}\sigma^{*}_{kl}\sigma^{*}_{ij}\mathrm{d}V,\end{aligned} \tag{1}$$

where $\overline{U}$ indicates the mean strain energy density in the representative volume element of concrete, ϵ' and $\sigma^{\star}$ indicate the virtual strain and the fictitious stress, respectively, E_{ij} indicates the average of ϵ', and H indicates the effective flexibility of concrete.

Likewise, the inequations with the idealized homogeneous stress boundary condition can be given as follows:

$$\begin{aligned}\overline{U} &\le \sum_{ij}\frac{1}{|\Omega|}\int_{\Omega}\epsilon'_{ij}\mathrm{d}V - \frac{1}{2|\Omega|}\int_{\Omega} L_{ijkl}\epsilon'_{kl}\epsilon'_{ij}\mathrm{d}V,\\ \overline{U} &\ge \frac{1}{2|\Omega|}\int_{\Omega} H_{ijkl}\sigma^{*}_{kl}\sigma^{*}_{ij}\mathrm{d}V.\end{aligned} \tag{2}$$

2.2.2. Voigt–Reuss Limit. According to the inequations obtained by the idealized homogeneous strain and stress boundary conditions, using the method introduced by Voigt and Reuss [40], the macroscopic elastic modulus can then be predicted.

Denoting the CAC as φ, the equivalent volume modulus and the equivalent shear modulus of concrete, k^{hom} and G^{hom}, can be expressed as

$$\frac{k_{\mathrm{cem}}k_{\mathrm{agg}}}{k_{\mathrm{agg}} - \varphi\left(k_{\mathrm{agg}} - k_{\mathrm{cem}}\right)} \le k^{\mathrm{hom}} \le k_{\mathrm{cem}} + \varphi\left(k_{\mathrm{agg}} - k_{\mathrm{cem}}\right), \tag{3}$$

$$\frac{G_{\mathrm{cem}}G_{\mathrm{agg}}}{G_{\mathrm{agg}} - \varphi\left(G_{\mathrm{agg}} - G_{\mathrm{cem}}\right)} \le G^{\mathrm{hom}} \le G_{\mathrm{cem}} + \varphi\left(G_{\mathrm{agg}} - G_{\mathrm{cem}}\right), \tag{4}$$

where k_{agg} and k_{cem} indicate the volume modulus of the aggregate and matrix, respectively, and G_{agg} and G_{cem} indicate the shear modulus of the aggregate and matrix, respectively.

2.2.3. Hashin–Shtrikman Limit. Furthermore, assuming the strain and stress are homogeneous on the segmented linear boundaries, a more precise group of upper and lower elastic modulus bounds, Hashin–Shtrikman limit, can be obtained [41]:

$$k^{\mathrm{hom}} \ge \frac{k_{\mathrm{cem}}\left(3k_{\mathrm{agg}} + 4G_{\mathrm{cem}}\right) + 4\varphi G_{\mathrm{cem}}\left(k_{\mathrm{agg}} - k_{\mathrm{cem}}\right)}{3k_{\mathrm{cem}} + 4G_{\mathrm{cem}} + 3\left(1-\varphi\right)\left(k_{\mathrm{agg}} - k_{\mathrm{cem}}\right)}, \tag{5}$$

$$G^{\mathrm{hom}} \ge \frac{6G_{\mathrm{cem}}G_{\mathrm{agg}}\left(k_{cem} + 2G_{\mathrm{cem}}\right) + G_{\mathrm{cem}}\left(9k_{\mathrm{cem}} + 8G_{\mathrm{cem}}\right)\left(\varphi G_{\mathrm{agg}} + (1-\varphi)G_{\mathrm{cem}}\right)}{G_{\mathrm{cem}}\left(9k_{\mathrm{cem}} + 8G_{\mathrm{cem}}\right) + 6\left(k_{\mathrm{cem}} + 2G_{\mathrm{cem}}\right)\left(\varphi G_{\mathrm{cem}} + (1-\varphi)G_{\mathrm{agg}}\right)}, \tag{6}$$

$$k^{\text{hom}} \leq \frac{k_{\text{cem}}\left(3k_{\text{cem}} + 4G_{\text{cem}}\right) + \varphi\left(k_{\text{agg}} - k_{\text{cem}}\right)\left(4G_{\text{cem}} - 3\left(k_{\text{agg}} - k_{\text{cem}}\right)\right)}{3k_{\text{cem}} + 4G_{\text{cem}} - 3\varphi\left(k_{\text{agg}} - k_{\text{cem}}\right)}, \tag{7}$$

$$\begin{aligned} G^{\text{hom}} \leq & \frac{5G_{\text{cem}}^2\left(3k_{\text{cem}} + 4G_{\text{cem}}\right)}{5G_{\text{cem}}\left(3k_{\text{cem}} + 4G_{\text{cem}}\right) - 6\varphi\left(k_{\text{cem}} + 2G_{\text{cem}}\right)\left(G_{\text{agg}} - G_{\text{cem}}\right)} \\ & + \frac{\varphi\left(G_{\text{agg}} - G_{\text{cem}}\right)\left(5G_{\text{cem}}\left(3k_{\text{cem}} + 4G_{\text{cem}}\right) - 6G_{\text{agg}}\left(k_{\text{cem}} + 2G_{\text{cem}}\right)\right)}{5G_{\text{cem}}\left(3k_{\text{cem}} + 4G_{\text{cem}}\right) - 6\varphi\left(k_{\text{cem}} + 2G_{\text{cem}}\right)\left(G_{\text{agg}} - G_{\text{cem}}\right)}. \end{aligned} \tag{8}$$

2.3. Numerical Simulation. The simulation in this study was implemented in three main steps: (1) generating the geometrical model based on RFM, (2) generating the mesh and assigning the material properties of each component, and (3) solving the finite element model.

2.3.1. Mesostructural Geometry. According to the self-similarity of a fractal, the simulation model of aggregates can be generated based on iteration. In this study, the convex hexahedron simulation model of aggregates was used. The convex hexahedron model was usually applied to create an approximate simulation of crushed stone as the aggregate. The basic generation algorithm of the convex hexahedron model can be described as follows:

(1) Dividing the cell: the cell is divided into several subauxiliary hexahedrons.

(2) Generating the aggregates: the subauxiliary hexahedron(s) at the specified location is(are) transformed to a real graph, and this real graph is treated as the model of an aggregate.

(3) Iteration: each remaining subauxiliary hexahedron is treated as a new cell, and steps 1 and 2 are repeated until the program ends.

More details about this numerical modeling method, such as setting and dividing the cells, definitions of the auxiliary and real graphs, and generation of aggregates at the specified locations, can be found in the papers reporting our previous studies [42, 43].

After generating the aggregates, the remaining space in the numerical concrete model can be treated as a matrix [44]. Simulation of the ITZ is discussed in Section 2.3.3.

A major advantage of RFM is that it involves the application of an index, i.e., the fractal dimension that can describe the geometric character of the concrete. Moreover, this iteration-based method provides an efficient numerical modeling technique.

2.3.2. Material Properties. As the strength of the aggregate is much greater than that of the matrix and ITZ, the aggregate model can be considered elastic. The constitutive behaviors of a matrix are formulated based on linear elastic damage mechanics, with the maximum tensile strain criterion as the threshold.

In particular, the mechanical properties and the gradation of the fine aggregates, as well as the air voids, will influence the mechanical behavior of concrete with no doubt. It can be demonstrated that its influence is on the matrix directly, and then the mechanical properties and portion of the matrix will influence the whole concrete. Limited by the calculation ability of a computer, the concrete was simulated at the mesolevel in this way: none of the fine aggregates nor the air voids would be represented separately. The effect of these composites was represented by the mechanical properties of the matrix. That is to say, all the fine aggregates and the air voids were considered a part of the matrix.

The constitutive law of the ITZ employed in this approach conforms to the failure criterion proposed in [1]. Denoting the shear and tensile strength of ITZ as f_s and f_t, respectively, the failure surface S_{failure} is given as the following three-parameter hyperbola:

$$S_{\text{failure}} = \tau^2 - \left(\sigma - f_s \tan\phi\right)^2 + \left(f_t - f_s \tan\phi\right)^2, \tag{9}$$

where τ is the shear stress; σ is the normal stress; and ϕ is the asymptotic friction angle, which is set as 27° according to the study in [1].

Several basic material properties of the three concrete components, including Young's modulus, Poisson's ratio, crack strain, f_s, and f_t, can be determined experimentally. The experimentation process and the results are given in Sections 3.2 and 4.1, respectively.

2.3.3. Mesh Generation and Assignment of Material Properties. A tetrahedron-shaped element, Solid65, was selected for use in this study. In order to mesh different geometrical models automatically, the SMRTSIZE command of ANSYS was employed. This command provides a manner of specified mesh generation with automatic (smart) element sizing, which could mesh the aggregate model with different sizes automatically. Commonly, the matrix was suggested to mesh based on the nodes of the element of the aggregate model. Then, the elements of aggregates and matrix can be assigned with their material properties, respectively.

The ITZ elements were generated according to the following method: Firstly, the nodes are selected on the interface between the aggregate and the matrix. Then, the elements attached to the selected nodes are selected and refined. Finally, the refined elements for the matrix attached to the nodes on the interface were assigned with material properties corresponding to the ITZ.

2.3.4. Model Solving. The numerical model in this study is solved in ANSYS by employing the ETABLE and EKILL

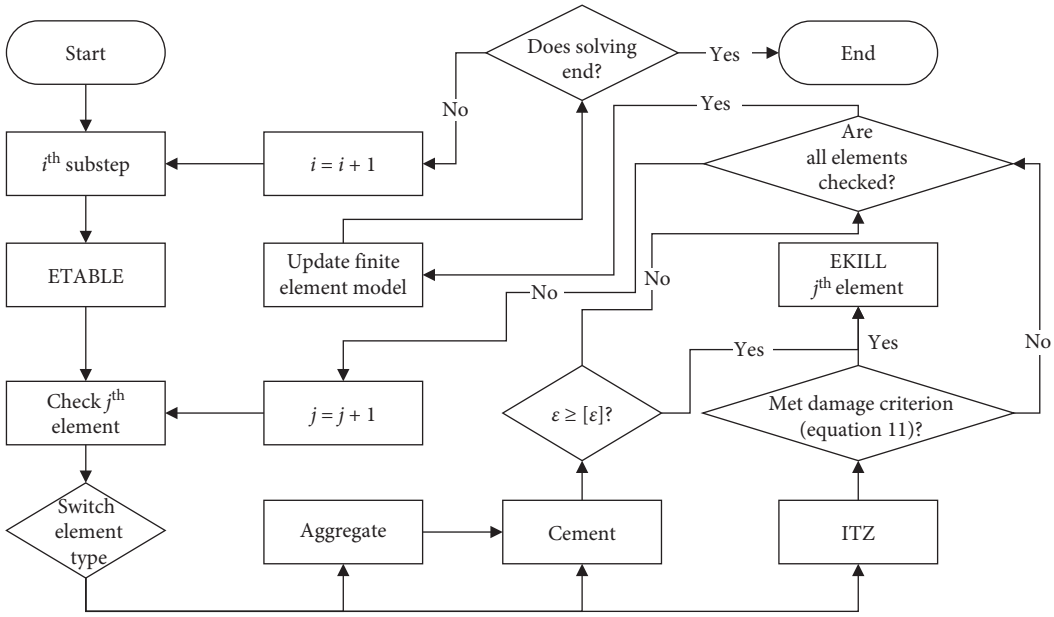

Figure 1: Schematic diagram of the algorithm for solving the finite element model.

commands. The algorithm used for solving the model is shown in Figure 1.

The ETABLE command can be executed to read various result data of each element for use in further processing. In this simulation, ETABLE was employed to read the strain, normal, and shear stress. Then, the damage of the element will be validated according to the criterion of damage. Once the damage criterion was met, the element will be "killed" by employing the EKILL command. The EKILL command was employed to simulate the damage of the element by deactivating an element. A deactivated element remains in the model but contributes a near-zero stiffness value to the overall matrix. This method can simulate quasibrittle materials efficiently.

3. Experiments and Simulations

Experiments were performed to determine the mechanical behavior of concrete prisms, as well as the material properties of composites.

3.1. Experiments with Concrete Prism. To discuss the influence of the fractal dimension of the matrix, three groups of concrete samples with varied gradations were prepared. Applying the calculation method introduced in [31], the fractal dimension of each gradation can be obtained. The sieving test results, as well as the fractal dimensions calculated for each group, are summarized in Table 1.

Each group contained six prism samples, and the dimensions of the prism are 150 mm × 150 mm × 300 mm. The CAC of all samples was set as 50%. The content of the other components was as follows: 195 kg/m^3 of water, 325 kg/m^3 of ordinary Portland cement of type 42.5R, and 696 kg/m^3 of sand were added, respectively.

All of the concrete prism samples were tested with a closed-loop, servo-controlled compression-testing machine with a capacity of 2000 kN. The stress-strain curves for each sample could then be obtained. The slope of the stress-strain curve in the linear regime could be used to calculate Young's modulus of the concrete samples.

Table 1: Sieving test results for the concrete prism samples.

Sieving level	Sieving size (mm)	Group 1 ($D = 2.3607$) SSR		Group 2 ($D = 2.4412$) SSR		Group 3 ($D = 2.5212$) SSR	
		(kg)	(%)	(kg)	(%)	(kg)	(%)
1	10	10.36	16.61	9.58	15.77	9.14	14.79
2	5	30.50	48.89	29.41	48.39	29.26	47.34
3	2.5	20.12	32.26	20.80	34.22	22.18	35.88

Note: SSR denotes separated sieve residue.

3.2. Experiments with Concrete Components. In this study, the main aim was to focus on the influence of the geometric properties of the mesostructure. Therefore, after tests to determine the mechanical parameters for each component, the average of each measurement was employed in the numerical model.

The following mechanical tests for determining the mechanical parameters of components were employed:

(1) Young's modulus and Poisson's ratio for the aggregate were tested by a group of cylindrical specimens drilled from the parent rock.

(2) Young's modulus, Poisson's ratio, and crack strain for the matrix were tested by a group of prism-shaped mortar specimens. The content of the mortar was as follows: 195 kg/m^3 of water, 325 kg/m^3 of ordinary Portland cement of type 42.5R, and 696 kg/m^3 of sand were added, respectively.

(3) The shear and tensile strength of the ITZ was tested by the specimens produced, as shown in Figures 2 and 3, respectively.

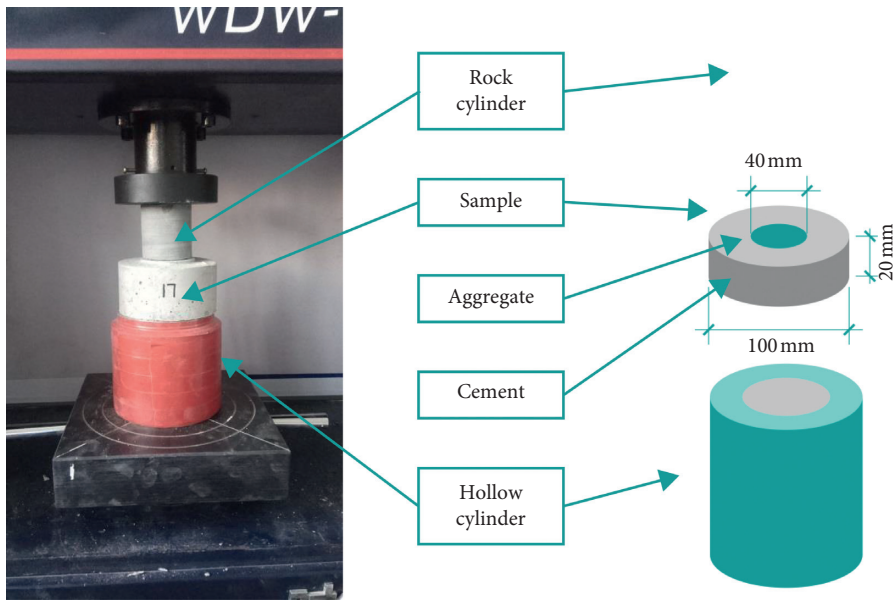

Figure 2: Setup for testing shear strength of the ITZ.

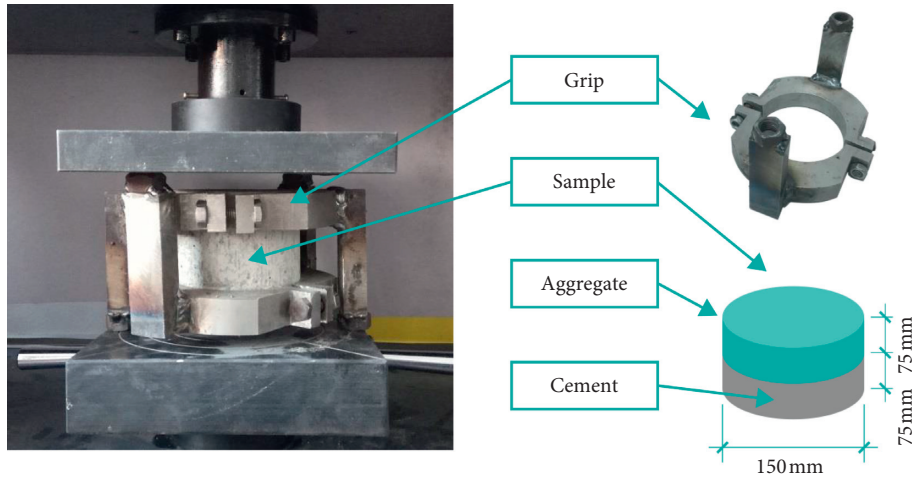

Figure 3: Setup for testing tensile strength of the ITZ.

More details about the experimentation, such as the setup of the test, the measurement, and setting of the gauge and linear variable differential transformers, can be found in the paper reporting our previous study [43].

3.3. Simulation. The main discussion of the effect of the geometric parameters of the numerical model, i.e., the fractal dimension of the matrix and the CAC, on the elastic modulus in this article is based on numerical simulations.

Before all, a validation of the simulation would be performed by comparison with experimental measurements. Three groups of prism-shaped numerical models with the same fractal dimension of the relevant concrete samples were analyzed. Each component model was assigned with the corresponding mechanical properties measured from the experiments introduced in Section 3.2. The results will be presented and discussed in Section 4.3.

Table 2: Various material parameters used for aggregates and matrix.

Component	Young's modulus (N/mm^2)	Poisson's ratio	Crack strain
Aggregates	5.35×10^4	0.23	—
Matrix	3.01×10^4	0.18	266×10^{-6}

Then, an orthogonal simulation study was designed. The fractal dimensions of models were set as 2.1, 2.2, ..., 2.9, and the CACs were set as 35%, 40%, ..., 70%. Each simulation model was generated based on these two parameters. A total of 72 concrete mesomodels with various fractal dimensions and CAC values were studied and discussed.

The naming conventions for these simulation models are as follows: D indicates the fractal dimension of the matrix,

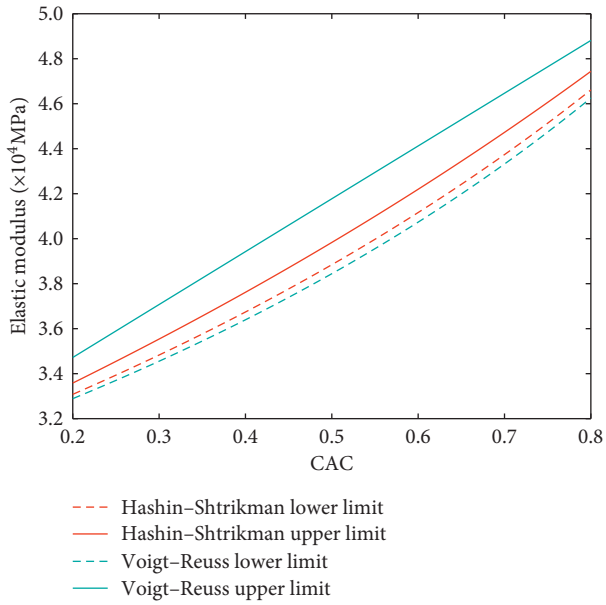

Figure 4: Effect of the CAC on analytical elastic modulus limits.

and the two sequent numbers indicate 10 times the fractal dimension value; P indicates the CAC of concrete, and the two sequent numbers indicate 100 times the CAC value. For instance, the simulation model D21P35 has a fractal dimension of 2.1 and the CAC of 35%.

Firstly, geometric models of the concrete prisms could be generated. By applying the measured mechanical parameters for each component, the aggregate was assigned with the corresponding material properties. The geometric model could then be meshed. Finally, the numerical mesomodels under compression could be solved in ANSYS using the method described in Section 2.3.4. The results are presented and discussed in Section 4.

4. Results and Discussion

4.1. Material Parameters of Each Component. The elastic parameters and elastic threshold of the matrix are listed in Table 2. Young's modulus of the ITZ was approximately set as 0.8 times Young's modulus of the matrix, and its Poisson's ratio was set as 0.2 [45, 46]. Besides, the air voids would be varied with the CAC and water-to-cement ratio change. It can be considered approximately that the material property of the mortar measured from the test could represent the influence of the pores.

The ITZ had a shear capacity of 2.72 MPa and a tensile capacity of 0.29 MPa. In reality, the rock cylinder used in the ITZ shear strength tests also contributed to the overall peak strength measured by the tests. However, because the stiffness of the rock is much higher than that of the ITZ, the contribution of the rock was neglected.

4.2. Discussion of Analytical Solution. Taking the mechanical parameters measured in tests to equations (3)–(7), the effect of the coarse aggregate on the effective modulus of concrete is shown in Figure 4.

A remarkable positive correlation could be observed between the analytical elastic modulus and the CAC. These relationships can be partly explained by the contribution of aggregates to the elastic modulus. In the elastic stage, the aggregate is a major factor determining the mechanical properties. A higher CAC usually results in a higher elastic modulus [47]; the analytical results confirm this conclusion.

Besides, it can be observed that the analytical solution can only describe the influence of the elastic modulus of components and the CAC on the concrete's elastic modulus. The influence of the matrix's fractal dimension or of the ITZ cannot be studied only according to the analytical solution.

4.3. Comparison of the Experimental and Simulation Results. The comparison of elastic modulus between the simulation results for each group and the corresponding experimental results is shown in Table 3.

It can be observed that there was little difference between the elastic modulus of the three groups of samples. Meanwhile, the simulation results matched the actual test results. Besides, the elastic modulus measured in the tests was slightly larger than that obtained with the simulation. This phenomenon would result in the numerical model having lower randomness than the actual concrete sample.

4.4. Effect of the Geometric Form of the Mesostructure on the Initial Elastic Modulus. Based on the simulation method introduced above, stress-strain curves could be obtained for the numerical mesomodels. The slope of the curve in the range between 0 and 0.5 MPa was defined as the initial elastic modulus of the numerical mesomodel.

The relationship between the fractal dimension and the initial elastic modulus is shown in Figure 5. A significant positive correlation was observed between the elastic modulus and the CAC. Meanwhile, the influence of the

Table 3: Comparison of simulation and experimental results.

Group number	Fractal dimension	Experimental results ($\times 10^4$ MPa)	Simulation results ($\times 10^4$ MPa)		
			Maximum	Minimum	Mean
1	2.3607	3.91	3.35	3.43	3.40
2	2.4412	3.54	3.49	3.65	3.57
3	2.5212	3.34	3.35	3.57	3.49

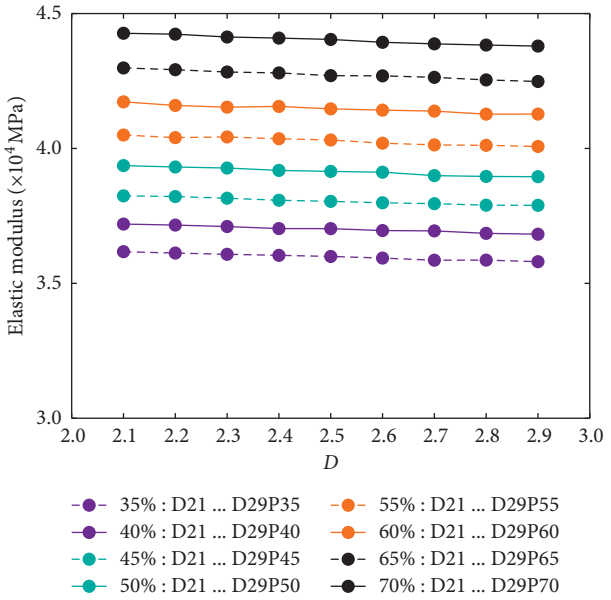

Figure 5: Effect of the geometric form of the mesostructure on the initial elastic modulus.

fractal dimension on the elastic modulus was quite small; increasing the fractal dimension resulted in a slight decrease in the elastic modulus.

The fractal dimension only has a direct effect on the geometric form of the matrix and the spatial distribution of aggregates. Based on the simulation results and observed experimental phenomena, the influence of these two factors on the elastic behavior may be slight.

5. Conclusions and Future Works

5.1. Conclusions. This study analyzed the effect of geometrical parameters, i.e., the fractal dimension of the matrix and the CAC, on the elastic modulus of concrete. The following conclusions can be drawn:

(1) The influence of fractal dimension on elastic modulus was quite small, which might cause the elastic modulus to decline slightly.

(2) With the increasing CAC, the elastic modulus increased.

This study contributes to our understanding of characterizing the geometrical form of the concrete mesostructure and its influence on the macroscopic behavior. The comprehensive consideration of the fractal geometry and classic Euclidean geometry can provide a powerful tool for understanding and predicting the observed macroscopic behavior.

Furthermore, a proper understanding of the fractal dimension of the concrete mesostructure can guide the study of other systems containing particulate solids with a rough surface. This study could provide some essential information that will help improve efficiency for structural engineers and researchers.

5.2. Future Works. Only the effect on the elastic parameters of concrete was studied in this paper based on the analytical method, experimentation, and simulation. Actually, concrete is a quasibrittle mixture with a complex mechanical behavior. The gradation and the spatial distribution of aggregates influence significantly the nonlinear regime and the cracking pattern. The study of the effect of the concrete mesostructure geometrical form on its mechanical behavior is still in the early stage. We would discuss the effect of the mesostructure on other behaviors at the macrolevel of concrete in our future works.

Data Availability

The experimental and simulation data used to support the findings of this study are included within the article.

Conflicts of Interest

The author declares that there are no conflicts of interest.

Acknowledgments

This work was supported by the China Postdoctoral Science Foundation Grant (Nos. 2019M651292 and 2019T120273).

References

[1] A. Caballero, C. M. López, and I. Carol, "3d meso-structural analysis of concrete specimens under uniaxial tension," *Computer Methods in Applied Mechanics and Engineering*, vol. 195, no. 52, pp. 7182–7195, 2006.

[2] Z. Chuhan, T. Xinwei, Z. Yuande, and J. Hui, "State-of-the-art literature review on concrete meso-scale mechanics," *Journal of Hydroelectric Engineering*, vol. 12, pp. 1–18, 2015.

[3] Y. Huang, Z. Yang, W. Ren, G. Liu, and C. Zhang, "3d meso-scale fracture modelling and validation of concrete based on in-situ x-ray computed tomography images using damage plasticity model," *International Journal of Solids and Structures*, vol. 67-68, pp. 340–352, 2015.

[4] E. J. Garboczi, "Three-dimensional mathematical analysis of particle shape using x-ray tomography and spherical

harmonics: application to aggregates used in concrete," *Cement and Concrete Research*, vol. 32, no. 10, pp. 1621–1638, 2002.

[5] Y. Xie, D. J. Corr, F. Jin, H. Zhou, and S. P. Shah, "Experimental study of the interfacial transition zone (itz) of model rock-filled concrete (rfc)," *Cement and Concrete Composites*, vol. 55, pp. 223–231, 2015.

[6] H. Dai and W. Wang, "Application of low-discrepancy sampling method in structural reliability analysis," *Structural Safety*, vol. 31, no. 1, pp. 55–64, 2009.

[7] M. Nitka and J. Tejchman, "A three-dimensional meso-scale approach to concrete fracture based on combined DEM with X-ray μCT images," *Cement and Concrete Research*, vol. 107, pp. 11–29, 2018.

[8] J. Suchorzewski, J. Tejchman, and M. Nitka, "Discrete element method simulations of fracture in concrete under uniaxial compression based on its real internal structure," *International Journal of Damage Mechanics*, vol. 27, no. 4, pp. 578–607, 2018.

[9] W. Xu, H. Ma, S. Ji, and H. Chen, "Analytical effective elastic properties of particulate composites with soft interfaces around anisotropic particles," *Composites Science and Technology*, vol. 129, pp. 10–18, 2016.

[10] Z. Weiping, W. Hao, and G. Xianglin, "Effects of randomly distributed aggregates on thermal properties of concrete," *Journal of Building Materials*, vol. 20, no. 2, pp. 168–173, 2017.

[11] X. Du, L. Jin, and G. Ma, "A meso-scale numerical method for the simulation of chloride diffusivity in concrete," *Finite Elements in Analysis and Design*, vol. 85, pp. 87–100, 2014.

[12] H. Dai and Z. Cao, "A wavelet support vector machine-based neural network metamodel for structural reliability assessment," *Computer-aided Civil and Infrastructure Engineering*, vol. 32, no. 4, pp. 344–357, 2017.

[13] W.-Q. Jiang, X.-H. Shen, J. Xia, L.-X. Mao, J. Yang, and Q.-F. Liu, "A numerical study on chloride diffusion in freeze-thaw affected concrete," *Construction and Building Materials*, vol. 179, pp. 553–565, 2018.

[14] F. Pan, F. Dang, Z. Ma, K. Jiao, and J. Shi, "Dynamic flexural mechanical properties and mechanism study of concrete beam specimens under different loading rates," *Journal of Investigative Medicine*, vol. 63, pp. S47–S48, 2015.

[15] J. Zheng, X. Zhou, and X. Jin, "An n-layered spherical inclusion model for predicting the elastic moduli of concrete with inhomogeneous itz," *Cement and Concrete Composites*, vol. 34, no. 5, pp. 716–723, 2012.

[16] Y. Ju, L. Wang, H. Xie et al., "Visualization of the three-dimensional structure and stress field of aggregated concrete materials through 3d printing and frozen-stress techniques," *Construction and Building Materials*, vol. 143, pp. 121–137, 2017.

[17] Z. P. Bažant and E. Becq-Giraudon, "Statistical prediction of fracture parameters of concrete and implications for choice of testing standard," *Cement and Concrete Research*, vol. 32, no. 4, pp. 529–556, 2002.

[18] X. Shiyun and Q. Qianqian, "Mesoscopic influence factor analysis on the equivalent elastic modulus of concrete," *Journal of Shenyang Jianzhu University: Natural Science*, vol. 4, pp. 636–643, 2015.

[19] I. Comby-Peyrot, F. Bernard, P.-O. Bouchard, F. Bay, and E. Garcia-Diaz, "Development and validation of a 3d computational tool to describe concrete behaviour at mesoscale. application to the alkali-silica reaction," *Computational Materials Science*, vol. 46, no. 4, pp. 1163–1177, 2009.

[20] D. Xiuli and J. Liu, "Applications of meso-scale analysis methods on the study of the physical/mechanical properties of concrete," *Journal of Hydraulic Engineering*, vol. 47, no. 3, pp. 355–371, 2016.

[21] M. Wang, A. Al-Tabbaa, and W. Wang, "Improving discrete particle packing models for the microstructural formation simulation of portland cement," *Construction and Building Materials*, vol. 229, Article ID 116841, 2019.

[22] M. Wang, Y. Liu, and W. Wang, "3d ca-lbm investigation of the interconnection of the platelet network within packed random porous structures," *Construction and Building Materials*, vol. 239, p. 117861, 2020.

[23] A. Yan, K.-R. Wu, D. Zhang, and W. Yao, "Effect of fracture path on the fracture energy of high-strength concrete," *Cement and Concrete Research*, vol. 31, no. 11, pp. 1601–1606, 2001.

[24] H. Dai, H. Zhang, and W. Wang, "A multiwavelet neural network-based response surface method for structural reliability analysis," *Computer-aided Civil and Infrastructure Engineering*, vol. 30, no. 2, pp. 151–162, 2015.

[25] A. P. N. Siregar, M. I. Rafiq, and M. Mulheron, "Experimental investigation of the effects of aggregate size distribution on the fracture behaviour of high strength concrete," *Construction and Building Materials*, vol. 150, pp. 252–259, 2017.

[26] B. B. Mandelbrot, *The Fractal Geometry of Nature*, Vol. 173, W. H. Freeman, New York, NY, USA, 1983.

[27] M. A. Issa, M. A. Issa, M. S. Islam, and A. Chudnovsky, "Fractal dimension--a measure of fracture roughness and toughness of concrete," *Engineering Fracture Mechanics*, vol. 70, no. 1, pp. 125–137, 2003.

[28] M. H. A. Beygi, M. T. Kazemi, I. M. Nikbin, J. Vaseghi Amiri, S. Rabbanifar, and E. Rahmani, "The influence of coarse aggregate size and volume on the fracture behavior and brittleness of self-compacting concrete," *Cement and Concrete Research*, vol. 66, pp. 75–90, 2014.

[29] H. Dai, B. Zhang, and W. Wang, "A multiwavelet support vector regression method for efficient reliability assessment," *Reliability Engineering & System Safety*, vol. 136, pp. 132–139, 2015.

[30] S. Khalilpour, E. BaniAsad, and M. Dehestani, "A review on concrete fracture energy and effective parameters," *Cement and Concrete Research*, vol. 120, pp. 294–321, 2019.

[31] X. Yang, R. Zhang, S. Ma, X. Yang, and F. Wang, "Fractal dimension of concrete meso-structure based on x-ray computed tomography," *Powder Technology*, vol. 350, pp. 91–99, 2019.

[32] P. Vargas, N. A. Marín, and J. I. Tobon, "Performance and microstructural analysis of lightweight concrete blended with nanosilica under sulfate attack," *Advances in Civil Engineering*, vol. 2018, Article ID 2715474, 11 pages, 2018.

[33] Y. Peng, Y. Wang, Q. Guo, and J. Ni, "Application of base force element method to mesomechanics analysis for concrete," *Mathematical Problems in Engineering*, vol. 2014, Article ID 528590, 11 pages, 2014.

[34] S. P. Ojha, S. Misra, A. Tinni, C. Sondergeld, and C. Rai, "Pore connectivity and pore size distribution estimates for wolfcamp and eagle ford shale samples from oil, gas and condensate windows using adsorption-desorption measurements," *Journal of Petroleum Science and Engineering*, vol. 158, pp. 454–468, 2017.

[35] H. Dai, G. Xue, and W. Wang, "An adaptive wavelet frame neural network method for efficient reliability analysis," *Computer-aided Civil and Infrastructure Engineering*, vol. 29, no. 10, pp. 801–814, 2014.

[36] H. Dai, H. Zhang, W. Wang, and G. Xue, "Structural reliability assessment by local approximation of limit state functions using adaptive Markov chain simulation and support vector regression," *Computer-Aided Civil and Infrastructure Engineering*, vol. 27, no. 9, pp. 676–686, 2012.

[37] K. Falconer, *Fractal Geometry - Mathematical Foundations and Applications*, John Wiley & Sons, Hoboken, NJ, USA, 1990.

[38] X. Yang, F. Wang, X. Yang, and Q. Zhou, "Fractal dimension in concrete and implementation for meso-simulation," *Construction and Building Materials*, vol. 143, pp. 464–472, 2017.

[39] A. U. Nilsen and P. J. Monteiro, "Concrete: a three phase material," *Cement and Concrete Research*, vol. 23, no. 1, pp. 147–151, 1993.

[40] R. Sakaguchi, B. Wiltbank, and C. Murchison, "Prediction of composite elastic modulus and polymerization shrinkage by computational micromechanics," *Dental Materials*, vol. 20, no. 4, pp. 397–401, 2004.

[41] Y. Peng, Q. Wang, L. Ying, M. M. A. Kamel, and H. Peng, "Numerical simulation of dynamic mechanical properties of concrete under uniaxial compression," *Materials*, vol. 12, no. 4, p. 643, 2019.

[42] X. Yang, F. Wang, X. Yang, F. Zhu, and B. Chi, "Quantity and shape modification for random-fractal-based 3d concrete meso-simulation," *Powder Technology*, vol. 320, pp. 161–178, 2017.

[43] X. Yang and H. Dai, "Effect of geometric form of concrete meso-structure on its mechanical behavior under compression," *Powder Technology*, vol. 360, pp. 372–382, 2020.

[44] L. C. Wang, "Meso-scale numerical modeling of the mechanical behavior of reinforced concrete members," *International Journal of Engineering and Technology*, vol. 5, no. 6, pp. 680–684, 2013.

[45] P. Sheng, Z. Chen, Y. Cui, J. Zhang, H. Zhang, and Z. Ji, "Numerical modeling of interfacial transition zone influence on elastic modulus of concrete," *Magazine of Concrete Research*, pp. 1–35, 2019.

[46] K. M. Lee and J. H. Park, "A numerical model for elastic modulus of concrete considering interfacial transition zone," *Cement and Concrete Research*, vol. 38, no. 3, pp. 396–402, 2008.

[47] L. K. Crouch, J. Pitt, and R. Hewitt, "Aggregate effects on pervious portland cement concrete static modulus of elasticity," *Journal of Materials in Civil Engineering*, vol. 19, no. 7, pp. 561–568, 2007.